BIT Numer Math (2009) 49: 449–473
DOI 10.1007/s10543-009-0222-3

BIT

Multirate infinitesimal step methods for atmospheric flow simulation

Jörg Wensch · Oswald Knoth · Alexander Galant

Received: 25 July 2008 / Accepted: 23 March 2009 / Published online: 4 April 2009

Abstract The numerical solution of the Euler equations requires the treatment of processes in different temporal scales. Sound waves propagate fast compared to advective processes. Based on a spatial discretisation on staggered grids, a multirate time integration procedure is presented here generalising split-explicit Runge-Kutta methods. The advective terms are integrated by a Runge-Kutta method with a macro stepsize restricted by the CFL number. Sound wave terms are treated by small time steps respecting the CFL restriction dictated by the speed of sound.

Split-explicit Runge-Kutta methods are generalised by the inclusion of fixed tendencies of previous stages. The stability barrier for the acoustics equation is relaxed by a factor of two.

Asymptotic order conditions for the low Mach case are given. The relation to commutator-free exponential integrators is discussed. Stability is analysed for the linear acoustic equation. Numerical tests are executed for the linear acoustics and the nonlinear Euler equations.

Keywords Runge Kutta methods · Multirate methods · Finite volume methods · Atmospheric dynamics

Communicated by Stig Skelboe.

This work was supported under the DFG priority program 1276, Metström: Multiple scales in fluid mechanics and meteorology.

J. Wensch (✉) · A. Galant
Fachrichtung Mathematik, Inst. f. wiss. Rechnen, TU Dresden, 01062 Dresden, Germany
e-mail: joerg.wensch@tu-dresden.de

A. Galant
e-mail: alexander.galant@tu-dresden.de

O. Knoth
Inst. f. Troposphärenforschung, Permoserstrasse 15, 04318 Leipzig, Germany
e-mail: knoth@tropos.de

Mathematics Subject Classification (2000) 65L06 · 65M12 · 76M12

1 Introduction

The efficient numerical simulation of instationary processes in science and engineering where processes on different timescales are coupled requires time integration procedures that deal with fast and slow components (or processes) in a different, adapted way. This approach has become popular in the ODE community under the name multirate time integration, see [8, 10, 20, 21].

In numerical weather prediction this approach is utilised under the name split-explicit methods. The Euler equations of gas dynamics in 1D formulated as balance equations of mass, momentum and energy admit wave solutions with three different characteristic velocities: the advective velocity u and sound waves propagated with velocities $u \pm c_s$. The stepsize of explicit integration methods is restricted by the CFL number corresponding to the sound wave velocity $|u| + c_s$. The pure advective process allows much larger timesteps. Typical maximum advective velocities in the lower to mid ranges of the troposphere are $u \approx 30$ m/s which is about $1/10$ of the speed of sound. Thus, in those regions the Euler equations form a system where slow and fast processes occur. We remark, that for a reliable numerical weather prediction the dynamics in the tropopause have to be predicted as well. There, jet streams may reach velocities of up to $1/3$ of the velocity of sound.

There are several approaches to deal with the fast waves, see [6] for an overview. Filtering of the basic equations completely eliminates or adds artificial damping to the sound waves. Between the full Euler equations and hydrostatic models there are the anelastic equations [14], pseudo-incompressible equations [5] and Boussineesq approximations [9] as non-hydrostatic models. Note, that these filtered equations may influence the dispersion relation for large scale phenomena like gravity waves, see [16]. Furthermore, filters can be applied to the spatial discretization via divergence damping, see [24]. This paper deals with the third alternative—to design time integration methods that can deal efficiently with fast waves.

Split-explicit methods integrate the advection terms with a large timestep of a Runge-Kutta- or multistep method where the stepsize is restricted by the CFL number of the advective velocity. The sound waves are treated by small time steps of a simpler method respecting the CFL-condition of the fast waves. In [24, 25] a multistage Runge-Kutta method in combination with forward-backward Euler is used.

When the stepsize for the fast waves tends to zero the fast wave equation is integrated exactly. Given

$$y'(t) = f(y(t)) + g(y(t)), \tag{1.1}$$

where f corresponds to the slow processes and g to the fast processes, we assume that the equation $y' = f(c) + g(y)$ or more general $y' = c + g(y)$ can be solved exactly. When g is linear, we arrive at the class of exponential integrators.

Splitting of the righthand-side in a (small) nonlinear part and a linear part $y' = N(y) + Ly$ is the base of a variety of methods that have been developed in very different application areas. The exact solution of $y' = c + Ay$, $y(0) = y_0$ is given by

$y(t) = \exp(tA)y_0 + t\phi(tA)c$, where $\phi(z) := (e^z - 1)/z$. The stability properties of exact solutions can be maintained for numerical solutions by different approaches. All these approaches require besides the approximation/evaluation of the exponential function and the function ϕ additionally the discussion of local and global order of accuracy of the methods.

First systematic investigations of higher order methods are given by Strehmel and Weiner [22, 23]. In their methods—adaptive Runge-Kutta methods—the exponential function is approximated by a rational function with suitable stability properties, whereas the order of the underlying Runge-Kutta method is preserved. Lubich and Hochbruck [11] use a Krylov-space approximation to the exponential function. Hochbruck and Ostermann [12] use the matrix exponential itself in their methods. Typical applications for these methods are either stiff problems or highly oscillatory differential equations.

A more general approach to splitting methods is obtained in the setting of differential equations on manifolds. The righthand-side of the differential equation is given by a vector field. For special vector fields it is assumed that the differential equation is exactly solvable—this is exactly our assumption on the equation $y' = f(c) + g(y)$. [15] give order conditions for a class of methods where multiple steps (exponentials) at each stage are allowed.

When a step from t_n to t_{n+1} is executed, the split-explicit methods of Wicker and Skamarock [25] start the exact integration procedure always at y_n. The exponential integrators of Celledoni et al. [4] start at the point y_n, too, but they allow for multiple exponentials in each stage. By these multiple exponentials their methods also include methods where the exact integration procedure starts at previously computed inner stages Y_{ni}. Methods based on such an approach have been investigated in [13], too. We generalise all these approaches by allowing for

- arbitrary starting points for the exact integration procedure based on previously computed internal stages
- a more general constant term $f(c)$ based on previously computed internal stages.

In order to make the method applicable to problems where the f- and g-terms in the righthand-sides are balancing each other, we aim for a numerical approach where this balance of f and g is respected (see next section, (2.3)). Unbalanced methods have been constructed by Gassmann [7] where small time step integration with pure g-terms is executed. These methods show improved stability properties compared with the methods of Wicker and Skamarock.

The remainder unfolds as follows. In Sect. 2 we define the method and give some basic properties. Section 3 is devoted to the derivation of order conditions. Stability properties of the method with respect to the acoustics equation are derived in Sect. 4. In Sect. 5 the construction of partitioned methods is outlined, and comparison with existing methods with respect to their stability region is given. Numerical experiments (Sect. 6) and conclusions end the paper.

2 The method

Given the partitioned equation

$$y'(t) = f(y(t)) + g(y(t)), \tag{2.1}$$

we assume that the equation $y' = c + g(y)$ where the tendencies c of the slow components are fixed is solved exactly. By that assumption we split the otherwise rather complicated investigation of order and stability into two steps. First, order and stability properties of the multirate infinitesimal step method are investigated. Second, in a practical implementation, the exact integration procedure is substituted by a numerical integration procedure of sufficiently high order and sufficiently good stability properties. The stability properties of the "finite step" version have to be reviewed afterwards.

A Runge-Kutta method for the integration of $y' = F(y)$ uses internal stages of type

$$Y_{ni} = y_n + h \sum_j a_{ij} F(Y_{nj}).$$

Such a stage can be interpreted as a method using exact integration of $y' = c$ via

$$\begin{aligned} Z_{ni}(0) &= y_n \\ Z'_{ni}(\tau) &= \sum_j a_{ij} F(Y_{nj}) \\ Y_{ni} &= Z_{ni}(h). \end{aligned}$$

The version above starts the exact integration procedure always at y_n. The methods of Knoth and Wolke [13] start the procedure always at $Y_{n,i-1}$. A generalisation of both is

$$\begin{aligned} Z_{ni}(0) &= y_n + h \sum_j \alpha_{ij} a_{ij} F(Y_{nj}) \\ Z'_{ni}(\tau) &= \sum_j (1 - \alpha_{ij}) a_{ij} F(Y_{nj}) \\ Y_{ni} &= Z_{ni}(h), \end{aligned}$$

where we start at some intermediate point.

We extend the concept above to a partitioned system with $F = f + g$ where $y' = c + g(y)$ can be solved exactly. In order to avoid the explicit evaluation of g we use linear combinations of $Y_{nj} - y_n$ instead of linear combinations of g-evaluations at the internal stages. In each stage a variable $Z_{ni}(\tau)$ is computed as the exact solution of $Z'(\tau) = c + g(Z(\tau))$.

Definition 2.1 A Multirate Infinitesimal Step method (MIS) is given by internal stages Y_{ni} defined by

$$Z_{ni}(0) = y_n + \sum_j \alpha_{ij}(Y_{nj} - y_n) \tag{2.2a}$$

$$\frac{\partial}{\partial \tau} Z_{ni}(\tau) = \frac{1}{h} \sum_j \gamma_{ij}(Y_{nj} - y_n) + \sum_j \beta_{ij} f(Y_{nj}) + d_i g(Z_{ni}(\tau)) \tag{2.2b}$$

$$Y_{ni} = Z_{ni}(h), \tag{2.2c}$$

where the update formula is given as stage number $s+1$ via $y_{n+1} = Y_{n,s+1}$. For $i \le j$ we have $\alpha_{ij} = \beta_{ij} = \gamma_{ij} = 0$. The method is balanced if

$$d_i = \sum_j \beta_{ij}. \tag{2.3}$$

Note, the first stage is $Y_{n1} = y_n$ as usual. By interpreting the update y_{n+1} as stage $s+1$, the stages and the final value y_{n+1} can be treated in a unified way. In this paper we restrict ourselves to balanced methods.

The following abbreviations will be used below:

$$(\boldsymbol{\alpha})_{ij} = \alpha_{ij}, \qquad (\boldsymbol{\beta})_{ij} = \beta_{ij}, \qquad (\boldsymbol{\gamma})_{ij} = \gamma_{ij},$$

$$C = \operatorname{diag}(c_1, \ldots, c_{s+1}), \qquad D = \operatorname{diag}(d_1, \ldots, d_{s+1}), \qquad \tilde{C} = \operatorname{diag}(\tilde{c}_1, \ldots, \tilde{c}_{s+1}),$$

$$Y = (Y_{n1}^T, \ldots, Y_{n,s+1}^T)^T, \qquad f(Y) = (f(Y_{n1})^T, \ldots, f(Y_{n,s+1}^T))^T, \text{ etc.},$$

$$\mathbb{1} = (1, \ldots, 1)^T, \qquad R = (I - \boldsymbol{\alpha} - \boldsymbol{\gamma})^{-1}, \qquad \tilde{b}^T = e_{s+1}^T R D, \qquad \tilde{c} = \boldsymbol{\alpha} c.$$

In matrix notation a MIS method is given as

$$Z(0) = \mathbb{1} \otimes y_n + (\boldsymbol{\alpha} \otimes I)(Y - \mathbb{1} \otimes y_n) \tag{2.4a}$$

$$\frac{\partial}{\partial \tau} Z(\tau) = \frac{1}{h} (\boldsymbol{\gamma} \otimes I)(Y - \mathbb{1} \otimes y_n) + (\boldsymbol{\beta} \otimes I) f(Y) + (D \otimes I) g(Z(\tau)) \tag{2.4b}$$

$$Y = Z(h) \tag{2.4c}$$

$$y_{n+1} = e_{s+1}^T Y. \tag{2.4d}$$

It is helpful to keep in touch with the explicit Runge-Kutta method that corresponds to the case $g = 0$. We use again the (slightly nonstandard) notation that the new approximation y_{n+1} is added as stage number $s+1$, i.e. the Runge-Kutta method is defined by a matrix $A \in \mathbb{R}^{(s+1)\times(s+1)}$. Nodes are given by $c = A\mathbb{1}$, where always $s_{s+1} = 1$.

Theorem 2.1 *When $g = 0$ the MIS method is equivalent to the application of an s-stage Runge-Kutta method to the equation $y' = f(y)$*

$$Y = \mathbb{1} \otimes y_n + h(A \otimes I) f(Y), \quad y_{n+1} = Y_{s+1}, \tag{2.5}$$

where the coefficient matrix A is given by

$$A = R\beta. \tag{2.6}$$

The nodes are $c = R\beta\mathbb{1} = RD\mathbb{1}$.

Proof Using the matrix notation above we obtain easily

$$\begin{aligned} Y = Z(h) &= Z(0) + hZ' \\ &= \mathbb{1} \otimes y_n + ((\boldsymbol{\alpha} + \boldsymbol{\gamma}) \otimes I)(Y - \mathbb{1} \otimes y_n) + h(\boldsymbol{\beta} \otimes I) f(Y) \\ \Rightarrow Y &= \mathbb{1} \otimes y_n + h(R\boldsymbol{\beta} \otimes I) f(Y). \end{aligned}$$

Therefore, the underlying explicit Runge-Kutta method has coefficient matrix $A = R\boldsymbol{\beta}$ and nodes $c = R\beta\mathbb{1} = RD\mathbb{1}$. □

3 Order conditions

For the special case $g = 0$ the classical order conditions for Runge-Kutta methods are obtained. In order to reproduce these conditions we use the matrix A from (2.6) instead of the coefficient matrix $\boldsymbol{\beta}$ in the order conditions. The numerical solution is expanded in a Taylor series. To this end we view Z_{ni} as a function of τ and h, both. We write shorthand

$$G(Y_{ni})^{(k)} := \left.\frac{\partial^k}{\partial h^k}\right|_{h=0} G(Y_{ni}), \qquad G(Z_{ni})^{(k,l)} := \left.\frac{\partial^{k+l}}{\partial \tau^k \partial h^l}\right|_{\tau=h=0} G(Z_{ni}). \tag{3.1}$$

We have easily

$$Y_{ni}^{(k)} = \sum_{l=0}^{k} \binom{k}{l} Z_{ni}^{(l,k-l)}. \tag{3.2}$$

The derivatives of Z are obtained as follows. Derivatives purely by h (type $(0, l)$) are obtained by differentiating the initial value (2.2a) of Z_{ni}. For derivatives of type $(1, l)$ we have to differentiate the righthand side of the differential equation (2.2b) l times with respect to τ. For derivatives of type (k, l), $k \geq 2$ the righthand side of the differential equation (2.2b) is differentiated at least once with respect to τ—therefore all τ-independent terms vanish. We end up with

$$\begin{aligned} Z_{ni}^{(0,l)} &= \sum_j \boldsymbol{\alpha}_{ij} Y_{nj}^{(l)} \\ Z_{ni}^{(1,l)} &= \frac{1}{l+1} \sum_j \gamma_{ij} Y_{nj}^{(l+1)} + \sum_j \beta_{ij} f(Y_{nj})^{(l)} + d_i g(Z_{ni})^{(0,l)} \\ Z_{ni}^{(k,l)} &= d_i g(Z_{ni})^{(k-1,l)}, \quad k \geq 2 \end{aligned}$$

or in matrix notation

$$Z^{(0,l)} = \boldsymbol{\alpha} Y^{(l)} \tag{3.3a}$$

$$Z^{(1,l)} = \frac{1}{l+1}(\boldsymbol{\gamma} \otimes I) Y^{(l+1)} + (\boldsymbol{\beta} \otimes I) f(Y)^{(l)} + (D \otimes I) g(Z)^{(0,l)} \tag{3.3b}$$

$$Z^{(k,l)} = (D \otimes I) g(Z)^{(k-1,l)}, \quad k \geq 2. \tag{3.3c}$$

Finally, the recursion for the derivatives of Y is given by

$$\begin{aligned} Y^{(k)} &= \sum_{l=1}^{k} \binom{k}{l} (D \otimes I) g(Z)^{(l-1,k-l)} \\ &\quad + ((\boldsymbol{\alpha} + \boldsymbol{\gamma}) \otimes I) Y^{(k)} + k(\boldsymbol{\beta} \otimes I) f(Y)^{(k-1)} \\ Y^{(k)} &= \sum_{l=1}^{k} \binom{k}{l} (RD \otimes I) g(Z)^{(l-1,k-l)} + k(A \otimes I) f(Y)^{(k-1)}. \end{aligned} \tag{3.4}$$

The recursion is initialised by (where $F = f + g$)

$$Y^{(0)} = Z^{(0,0)} = \mathbb{1} \otimes y_n \tag{3.5a}$$

$$\begin{aligned} Y^{(1)} &= (RD\mathbb{1} \otimes I) g + (A\mathbb{1} \otimes I) f \\ &= (c \otimes I) F \end{aligned} \tag{3.5b}$$

$$Z^{(0,1)} = (\boldsymbol{\alpha} c \otimes I) F = \tilde{c} \otimes F \tag{3.5c}$$

$$\begin{aligned} Z^{(1,0)} &= (\boldsymbol{\gamma} c \otimes I) F + (\boldsymbol{\beta}\mathbb{1} \otimes I) f + (D\mathbb{1} \otimes I) g \\ &= ((\boldsymbol{\gamma} + R^{-1}) c \otimes I) F = ((I - \boldsymbol{\alpha}) c \otimes I) F = (c - \tilde{c}) \otimes F. \end{aligned} \tag{3.5d}$$

With (3.4) we obtain expansions for higher order derivatives of y

$$\begin{aligned} Y^{(2)} &= 2(A \otimes I) f(Y)^{(1)} + (RD \otimes g_y)(2Z^{(0,1)} + Z^{(1,0)}) \\ &= 2Ac \otimes f_y F + RD(c + \tilde{c}) \otimes g_y F \\ Z^{(0,2)} &= (\boldsymbol{\alpha} \otimes I) Y^{(2)} \\ Z^{(1,1)} &= 1/2(\boldsymbol{\gamma} \otimes I) Y^{(2)} + \boldsymbol{\beta} c \otimes f_y F + D\tilde{c} \otimes g_y F \\ Z^{(2,0)} &= (D \otimes I) g(Z)^{(1,0)} = D(c - \tilde{c}) \otimes g_y F. \end{aligned}$$

We end up with the third-order derivative of Y

$$\begin{aligned} Y^{(3)} &= (RD \otimes I)(3g(Z)^{(0,2)} + 3g(Z)^{(1,1)} + g(Z)^{(2,0)}) + 3(A \otimes I) f(Y)^{(2)} \\ &= 3RD(\boldsymbol{\alpha} + \boldsymbol{\gamma}/2) \otimes g_y Y^{(2)} + 3(A \otimes I) f_y Y^{(2)} \\ &\quad + 3RD\boldsymbol{\beta} c g_y f_y F + 3Ac^2 \otimes f_{yy}(F, F) + RDD(c - \tilde{c}) g_y g_y F \\ &\quad + (3RD(\tilde{c}, \tilde{c}) + 3RD(\tilde{c}, c - \tilde{c}) + RD(c - \tilde{c}, c - \tilde{c})) \otimes g_{yy}(F, F) \end{aligned}$$

$$
\begin{aligned}
&= 3RD(I+\boldsymbol{\alpha})Ac \otimes g_y f_y F \\
&\quad + \left[3RD(\boldsymbol{\alpha}+\boldsymbol{\gamma}/2)RD(c+\tilde{c}) + RDD(c+2\tilde{c})\right] \otimes g_y g_y F \\
&\quad + 6AAc \otimes f_y f_y f + 3ARD(c+\tilde{c}) f_y g_y F \\
&\quad + 3Ac^2 \otimes f_{yy}(f,f) \\
&\quad + (RDc^2 + RD\tilde{c}^2 + RD(c,\tilde{c})) \otimes g_{yy}(F,F).
\end{aligned}
$$

Comparing with the expansion of the exact solution we obtain the well-known classical order conditions for order three

$$b^T \mathbb{1} = 1, \qquad b^T c = 1/2, \qquad b^T c^2 = 1/3, \qquad b^T Ac = 1/6 \tag{3.6}$$

and 1 additional order condition for order two

$$\tilde{b}^T (c+\tilde{c}) = 1 \tag{3.7}$$

and 4 additional order conditions for order three

$$\tilde{b}^T (I+\boldsymbol{\alpha})Ac = 1/3 \tag{3.8}$$

$$3\tilde{b}^T (\boldsymbol{\alpha}+\boldsymbol{\gamma}/2)RD(c+\tilde{c}) + \tilde{b}^T D(c+2\tilde{c}) = 1 \tag{3.9}$$

$$b^T RD(c+\tilde{c}) = 1/3 \tag{3.10}$$

$$\tilde{b}^T (c^2 + \tilde{c}^2 + c\cdot\tilde{c}) = 1. \tag{3.11}$$

4 Interpretation as exponential integrator

Celledoni et al. [4] developed commutator free integrators. We give a short sketch of the framework.

A differential equation on a differentiable manifold M is given by

$$y'(t) = v(y(t))|_{y(t)},$$

where $y(t) \in M$ and $v(y)$ is a vector field on M, i.e. v maps the manifold into the class of sufficiently smooth vector fields on M. Note, that y occurs twice on the righthand-side because the vector field $v(y)$ specifies tangent vectors $v(y)|_x$ at each point $x \in M$.

Points on a n-dimensional manifold are defined with respect to local coordinate systems, where each coordinate system $(x_1, \ldots, x_n)$ admits canonical vector fields $\partial x_1, \ldots, \partial x_n$. There are two interpretations of the vector field ∂x_i: it is either the derivative of a curve $x(t) \in M$ with

$$x_j(t) = \begin{cases} x_j(0) + t & \text{for } j = i \\ \text{const.} & \text{for } j \neq i \end{cases}$$

or the directional derivative $\frac{\partial f}{\partial x_i}$ of a smooth function $f : M \to \mathbb{R}$.

Canonical vector fields are generalised by the concept of frames. A system of frames $F_1, \ldots, F_d$, $d \geq n$, is a system of smooth vector fields that span the tangential space $TM|_x$ at each point $x \in M$. The righthand side $v(y)$ of the differential equation is represented by frames via

$$v(y)|_x = \sum_{i=1}^{d} v_i(y, x)\ F_i|_x\,.$$

The coefficients $v_i(y, x)$ are not uniquely determined in the case $n < d$. A complete system of frames has the property that differential equations

$$x'(t) = \sum_{i=1}^{d} v_i\ F_i|_{x(t)}$$

with constant coefficients v_i can be solved exactly. The exact solution is formally given by the exponential of the vector field

$$x(t) = \exp\left(t \sum_{i=1}^{n} v_i F_i\right) x(0).$$

The concept of frames is easily extended to our application: on the differentiable manifold $\mathbb{R}^n$ we choose $d = n + 1$ frames, where $F_1, \ldots, F_n$ span $\mathbb{R}^n$ and F_{n+1} is given by the function g:

$$\begin{aligned} F_i|_x &= \mathbf{e}_i = \begin{pmatrix} 0 & \ldots & 0 & 1 & 0 & \ldots & 0 \end{pmatrix}^T, \quad i = 1, \ldots, n \\ F_{n+1}|_x &= g(x). \end{aligned}$$

The righthand-side is evaluated at intermediate stages, the coefficients are frozen to obtain a righthand-side spanned by the frames, and the solution operator (exponential map) is applied to this vector field. We consider exponential integrators in the form

$$\begin{aligned} Y_1 &= y_n \\ Y_i &= \exp\left(h \sum_j a_{ij} \sum_k v_k(Y_j, Y_j) F_k\right) Y_{j(i)}, \quad i = 2, \ldots, s+1, \\ y_{n+1} &= Y_{s+1}, \end{aligned}$$

where the update formula has the same structure as the internal stages. The method is explicit when $a_{ij} = 0$ for $i \leq j$. Note, that in stage i the exact solution operator is applied to a previously computed internal stage $Y_{j(i)}$.

The class of exponential integrators described above fits in our framework of MIS methods by setting

$$\boldsymbol{\gamma} = 0, \quad \alpha_{ij} = \begin{cases} 1 & \text{for } j = j(i) \\ 0 & \text{otherwise,} \end{cases} \quad \beta_{ij} = a_{ij}, d_i = \sum_j a_{ij}.$$

They further belong to the class of methods developed in [4] where the successive application of multiple exponentials on the initial value y_n is allowed.

Therefore, these methods form the common subset of the exponential integrators of [4] and our methods. For further development in the class of commutator-free exponential integrators with application to advection-diffusion problems, see [2, 3]. There, in contrast to our application, the advective processes are treated by exponential integrators.

5 Stability of methods designed for numerical weather prediction

The dynamic core of weather prediction codes requires the solution of the Euler equations. Phenomena on different time scales occur—sound waves propagate fast compared to advective processes.

5.1 The stability function

We apply the method to the linear test problem

$$y' = \mu y + \lambda y,$$

i.e. $f(y) = \mu y$, $g(y) = \lambda y$. The exact solution of the initial value problem

$$y' = c + \lambda y, \qquad y(0) = y_0$$

is given by

$$y(t) = \exp(\lambda t) y_0 + t\phi(\lambda t)c, \qquad \phi(z) := (e^z - 1)/z.$$

The amplification of the numerical solution $y_{n+1} = R(h\mu, h\lambda)y_n$ is described by the stability function R. In matrix notation R is derived via

$$Y_n = \exp(h\lambda D)(\mathbb{1}y_n + \boldsymbol{\alpha}(Y_n - \mathbb{1}y_n)) + \phi(h\lambda D)(\boldsymbol{\gamma}(Y_n - \mathbb{1}y_n) + h\mu\boldsymbol{\beta}Y_n) \tag{5.1}$$

$$R(h\mu, h\lambda) = e_{s+1}^T (I - \exp(h\lambda D)\boldsymbol{\alpha} - \phi(h\lambda D)\boldsymbol{\gamma} - h\mu\phi(h\lambda D)\boldsymbol{\beta})^{-1} \times (\exp(h\lambda D)(I - \boldsymbol{\alpha})\mathbb{1} - \phi(h\lambda D)\boldsymbol{\gamma}\mathbb{1}). \tag{5.2}$$

The stability function for an infinite number of small steps serves to evaluate multirate methods a priori without specifying the number of small steps taken. Surely, for a finite number of small steps used in a practical implementation the stability properties of the method have to be reviewed.

5.2 Stability for linear acoustics

The simplest equation admitting both advection and propagation of sound waves are the linearised acoustics equations in 1D

$$u_t + U u_x = -c_s \pi_x$$
$$\pi_t + U \pi_x = -c_s u_x,$$

where $c_s = \sqrt{(\gamma - 1)c_p\theta}$ is the speed of sound, $\gamma = c_p/c_v$ and $\kappa = R/c_p$ are the adiabatic constants, c_p, c_v are the specific heat coefficients for expansion with constant pressure/volume. The background state is given by a constant potential temperature θ, reference pressure p_{ref}, and advection velocity U. $\pi = c_s/(\gamma - 1)(p/p_{ref})^{\kappa}$ is a weighted perturbation Exner pressure. The system exhibits waves propagating with velocities $U \pm c_s$.

Several established operating weather prediction codes use a spatial discretisation based on staggered grids (Arakawa C-grid [1]), see ICON, WRF, [7, 17–19, 24, 25]. Advection is discretised by third (or higher) order upwind-differences, whereas the terms responsible for sound waves are discretised by symmetric differences.

The procedures RK2/RK3 utilised in the WRF code use an underlying two/three-stage Runge-Kutta method for the advection terms and the so-called forward-backward Euler method for the integration of the sound waves.

Applying a von Neumann stability analysis, we substitute a wave with wave number k via $u(t, x) = u_k(t)\exp(ikx)$, $\pi(t, x) = \pi_k(t)\exp(ikx)$ in the acoustics equation to obtain for constant wave number k on a grid of gridwidth Δx, where subscript k is omitted,

$$u'(t) = -\frac{U}{\Delta x}a(z)u(t) - \frac{c_s}{\Delta x}s(z)\pi(t) \tag{5.3}$$

$$\pi'(t) = -\frac{U}{\Delta x}a(z)\pi(t) - \frac{c_s}{\Delta x}s(z)u(t) \tag{5.4}$$

with $z = \exp(ik\Delta x)$ and the discretisations $a(z)$ for advection (third order upwind) and $s(z)$ for symmetric differences on staggered grids for the sound waves are given by

$$a(z) = \frac{2z + 3 - 6z^{-1} + z^{-2}}{6}$$

$$s(z) = \sqrt{z}^{-1} - \sqrt{z}.$$

Equation (5.3) admits a diagonalisation where the sound wave term admits eigenvalues $\pm c_s/\Delta x s(z)$. In order to discuss stability of our methods for fixed Courant numbers $C_A = U\Delta t/\Delta x$, $C_S = c_s\Delta t/\Delta x$ with respect to advection velocity and speed of sound, we have to investigate

$$R_a(C_A, C_S) := \max_{k\in[0,\pi]} |R(C_A a(e^{ik}), \pm C_S s(e^{ik}))|.$$

The stability region S is then given by $S := \{(C_A, C_S) : R_a(C_A, C_S) \le 1\}$.

Finally, we will discuss the case when a finite number of small time steps is applied. Suppose, in stage i we apply n_i small time steps with stepsize $d_i h/n_i$ to the linear equation $y' = c + \lambda y$ with initial value $y(0) = y_0$.

When the small time step integrator is the explicit Euler method the stability function of the procedure is easily obtained. In case of $n_i = m$ small steps in each stage we simply replace the exponential and the function ϕ in (5.1) by

$$\exp(z, m) := (1 + z/m)^m, \qquad \phi(z, m) := (\exp(z, m) - 1)/m.$$

Also when different numbers of small steps are used in different stages, an explicit representation of the stability function can be derived. Here, we use the forward-backward Euler method. An explicit formula for the stability function becomes more complicated because the components u, π are integrated by different formulas. Especially, the stability function can not be stated as a polynomial in $C_A a(z)$ and $C_S s(z)$. In order to determine the stability regions, we preferred to set up the amplification matrix for the system (by execution of the method) and to compute its eigenvalues.

5.3 Review of known methods

5.3.1 Wicker-Skamarock

The methods of Wicker and Skamarock [25] are given by $\boldsymbol{\alpha} = \boldsymbol{\gamma} = 0$, so the small time step integration starts always at time level t_n. Their methods RK2 and RK3 are given by the Butcher tableaus

$$\begin{array}{c|cc} 0 & & \\ 1/2 & 1/2 & \\ \hline & 0 & 1 \end{array} \qquad \begin{array}{c|ccc} 0 & & & \\ 1/3 & 1/3 & & \\ 1/2 & 0 & 1/2 & \\ \hline & 0 & 0 & 1 \end{array}.$$

Note, that RK2 has order 2, also for the time-split version, whereas RK3 has order 3 only for linear equations. Methods with $\boldsymbol{\alpha} = \boldsymbol{\gamma} = 0$ have at most order 2 for the time-split version (assuming exact integration of the fast process) because order condition (3.8) reduces to $\sum_i b_i c_i = 1/3$ which contradicts the classical order condition $\sum_i b_i c_i = 1/2$.

5.3.2 Knoth-Wolke methods

Knoth and Wolke [13] use $\boldsymbol{\gamma} = 0$ and $\alpha_{i,i-1} = 1$ for $i = 2, \ldots, s+1$. Therefore, small time step integration in stage i starts at the previously computed stage $Y_{n,i-1}$.

The corresponding Butcher tableau of the underlying Runge-Kutta method (called KW3 here) is given by

$$\begin{array}{c|ccc} 0 & & & \\ 1/3 & 1/3 & & \\ 3/4 & -3/16 & 15/16 & \\ \hline & 1/6 & 3/10 & 8/15 \end{array}.$$

5.3.3 Exponential integrators

We have implemented the method of order 3 based on the method of Heun with

$$\boldsymbol{\alpha} = \begin{pmatrix} 0 & & & \\ 0 & 0 & & \\ 0 & 0 & 0 & \\ 0 & 1 & 0 & 0 \end{pmatrix}, \qquad \boldsymbol{\gamma} = 0, \qquad A = \begin{pmatrix} 0 & & & \\ 1/3 & 0 & & \\ 0 & 2/3 & 0 & \\ 1/4 & 0 & 3/4 & 0 \end{pmatrix}.$$

This method is denoted by CF3 in [15] and also in this paper.

5.3.4 Simplified order conditions

Knoth and Wolke [13] and Owren [15] found no additional order conditions for order 2, and one additional order condition for order 3. We generalise both methods to

Definition 5.1 A method has property A if $\boldsymbol{\gamma} = 0$, $\alpha_{ij} \in \{0, 1\}$, $\sum_j \alpha_{ij} \in \{0, 1\}$.

Theorem 5.1 *Under property A there are no additional order conditions for order two, and one additional order condition for order* 3, *namely* (3.8).

Proof First, property A implies both

$$\tilde{c}^k = \boldsymbol{\alpha} c^k \text{ and}$$
$$D = C - \tilde{C}.$$

We have conditions (3.7) and (3.11) implied via

$$\begin{aligned}\tilde{b}^T(c + \tilde{c}) &= e_{s+1}^T R(C - \tilde{C})(c + \tilde{c}) = e_{s+1}^T R(c^2 - \tilde{c}^2)\\ &= e_{s+1}^T (I - \boldsymbol{\alpha})^{-1}(I - \boldsymbol{\alpha})c^2 = c_{s+1}^2 = 1\\ \tilde{b}^T(c^2 + c\tilde{c} + \tilde{c}^2) &= e_{s+1}^T R(C - \tilde{C})(c^2 + c\tilde{c} + \tilde{c}^2) = e_{s+1}^T R(c^3 - \tilde{c}^3)\\ &= e_{s+1}^T (I - \boldsymbol{\alpha})^{-1}(I - \boldsymbol{\alpha})c^3 = c_{s+1}^3 = 1.\end{aligned}$$

Condition (3.9) is fulfilled via

$$\begin{aligned}&3\tilde{b}^T(\boldsymbol{\alpha} + \boldsymbol{\gamma}/2)RD(c + \tilde{c}) + \tilde{b}^T D(c + 2\tilde{c})\\ &= 3e_{s+1}^T RD\boldsymbol{\alpha} c^2 + e_{s+1}^T RD(c^2 + c\tilde{c} - 2\tilde{c}^2)\\ &= e_{s+1}^T RD(c^2 + c\tilde{c} + \tilde{c}^2) = 1.\end{aligned}$$

Finally, we have condition (3.10) fulfilled:

$$b^T RD(c + \tilde{c}) = b^T (I - \boldsymbol{\alpha})^{-1}(c^2 - \tilde{c}^2) = b^T c^2 = 1/3. \qquad \square$$

For methods of order 3 with property A we have one additional order condition, namely (3.8). This condition proves to be equivalent to the condition obtained in the special case of the Knoth/Wolke methods ($\alpha_{i,i-1} = 1$). The extra condition for third order exponential integrators (condition (26b) from [15]) reads in our notation

$$\sum_j a_{Kj} c_j + \frac{1}{2} \sum_j \beta_{s+1,j} = \frac{1}{3}, \tag{5.5}$$

where K is defined by $\alpha_{s+1,K} = 1$. Formula (5.5) proves easily equivalent to the remaining order condition (3.8).

5.4 Construction of partitioned methods

Our aim is to construct a three-stage method of order three. We parametrise the method by $c_2, c_3, \alpha_{32}, \tilde{c}_4$.

The underlying RK-method is completely determined by c_2, c_3, when the case $c_2 = 2/3$ is excluded.

By prescribing further α_{32} and $\tilde{c}_4$ the remaining parameters are completely determined. We have $\tilde{b}^T \mathbb{1} = e_4^T RD\mathbb{1} = e_4^T RR^{-1}c = 1$ and $\tilde{b}_1 = 1$. Therefore, $\tilde{b}$ is determined by the latter restriction and order conditions (3.7) and (3.11). With $s_{ij} := \alpha_{ij} + \gamma_{ij}$, we have s_{32} determined from condition (3.10). Then, we determine s_{42}, s_{43} from the values of $\tilde{b}^T$. α_{43} is determined from condition (3.8). Finally, α_{42} is determined from $\tilde{c} = \alpha c$.

It remains to satisfy condition (3.9). Eliminating all dependent parameters from (3.9) yields a complex nonlinear equation in the 4 variables $c_2, c_3, \alpha_{32}, \tilde{c}_4$ which has to be solved numerically.

In order to find methods with improved stability properties, we followed two approaches:

- We used a genetic optimisation procedure, where we tried to find coefficient sets where all coefficients are positive. This approach did not succeed.
- We determined several hundred coefficient sets satisfying the order conditions and reviewed the stability regions by visual inspection. From that approach we obtained several methods having improved stability properties compared with RK3. We have chosen two of them for numerical experiments, namely MIS3A and MIS3B.

The coefficients are given with 16 digit accuracy in the appendix. The forward-backward Euler method is applied as small time step integration procedure. Note, that our methods have some slightly negative coefficients. Nevertheless, their stability properties for the acoustics equation turned out to be favourable compared with RK3 and other methods. Further, even in a nonlinear test example, where the stability properties on a linear test equation serve only as heuristics, they turned out to allow larger stepsizes than the established methods.

5.5 Stability regions

We give here an overview on the stability regions when the linear test equation is given by the acoustics equation, discretised in space by third order upwind (advection) and central differences on a staggered grid (sound wave terms).

In order to analyse stability, it seems natural to favourise methods that have a large stability region for an infinite number of small steps (MIS). Thus there is no small time step size defined yet. The CFL number with respect to sound is therefore defined with respect to the macro step size

$$C_S = c_s \Delta t / \Delta x, \tag{5.6}$$

which is in contrast to the more common convention to display results with respect to the small step CFL number $C'_S = c_s \Delta\tau / \Delta x$, see [7, 24, 25].

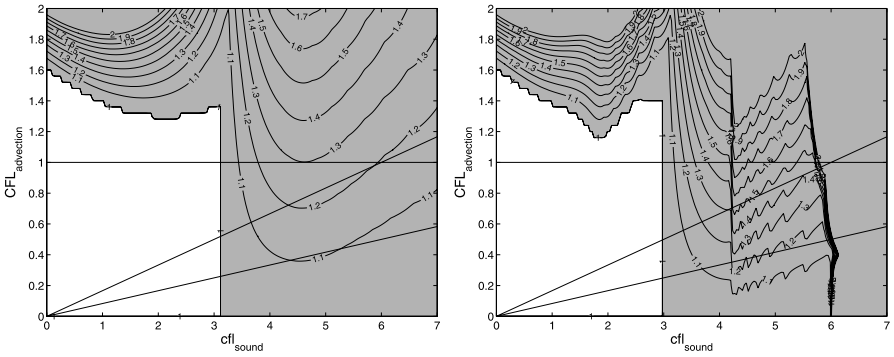

Fig. 1 Stability regions for RK3 with exact integration (*left*) and stepsequence [2, 3, 6] (*right*). Axis are CFL numbers with respect to macro step size Δt

When methods with promising stability region for MIS are identified, the finite step case is investigated. In each stage i, $i = 2, \ldots, s$, the number of forward-backward Euler steps n_i has to be fixed. We base a reasonable first guess on the assumption that the (effective) small time step $\Delta\tau_i = d_i/n_i \Delta t$ is restricted by the maximum CFL number 2 of the forward-backward Euler method. A save upper bound for the C_S-values inside the stability region (for MIS) is given by $C_S \leq 12$, see left images in Figs. 1 to 6. We obtain

$$2 \geq \Delta\tau_i c_s/\Delta x = \frac{d_i}{n_i} C_S \tag{5.7}$$

$$\Rightarrow n_i \geq 6 d_i. \tag{5.8}$$

In case of RK3 this leads to the commonly used sequence $[n_2, n_3, n_4] = [2, 3, 6]$. For the first guess we check whether the stability region occupies most of the stability region for the MIS case. Otherwise the values n_i are increased.

The Figs. 1 to 6 show the stability regions of RK3, MIS3A, MIS3B, CF3, KW3. The left hand images show stability for an infinite number of small time steps, whereas the right hand images show stability for a fixed number of small time steps. For convenience the lines $C_A = 1$, $C_A = 1/6 C_S$, $C_A = 1/12 C_S$ are drawn in all images. Assuming that advective velocities are bounded by μc_S, we are interested in methods being stable in the triangular region $C_A \leq \mu C_S$, where μ is determined by the speed of sound and typical advective velocities.

For fixed ratio $U/c_s \in \{1/6, 1/12\}$ the stability restriction on the macro time step CFL number $C_S = c_s \Delta t/\Delta x$ is displayed in Table 1.

5.6 Divergence damping

Acoustic waves pose a severe restriction to the time step size for the simulation of atmospheric dynamics by explicit methods. We want to point out that there are alternatives besides constructing methods where these restrictions are weakened.

Divergence damping is a simple but effective technique to combine sound wave filtering with split-explicit methods. A diffusive term depending on the deviation of

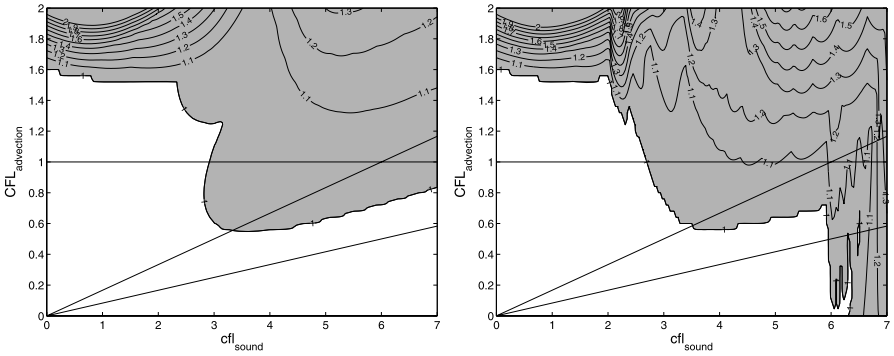

Fig. 2 Stability regions for MIS3A with exact integration (*left*) and stepsequence [3, 4, 6] (*right*). Axis are CFL numbers with respect to macro step size Δt

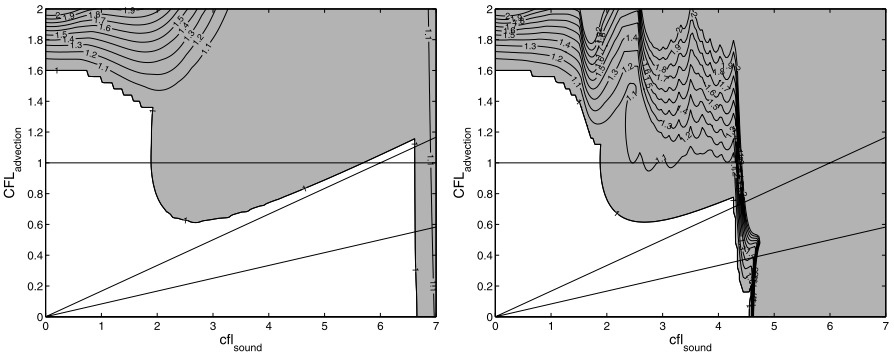

Fig. 3 Stability regions for MIS3Ba with exact integration (*left*) and stepsequence [2, 3, 4] (*right*). Axis are CFL numbers with respect to macro step size Δt

Table 1 Bounds on the macro time step CFL number for fixed ratio U/c_s

Method	$U/c_s = 1/6$	$U/c_s = 1/12$
RK3	3	3
MIS3A	3	6
MIS3Ba	4.5	4.5
MIS3Bb	6	6
CF3	2.3	2.4
KW3	2.5	2.3

divergence free flow is added to the balance of inertia. The stability barrier $C_S \leq 3$ for RK3 can be broken by that approach. For a detailed description we refer to [24]. The stability constraints for the fast and slow components are decoupled. The damping of sound waves shifts the eigenvalues of the sound modes from the imaginary axis to the left—thus the modulus of the exact amplification function is less than 1. Therefore,

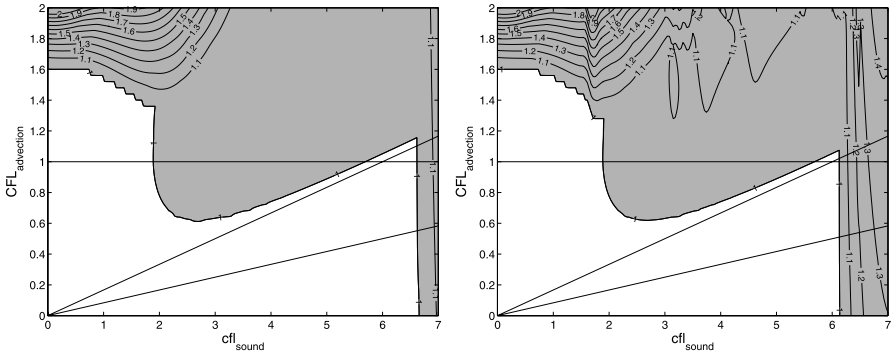

Fig. 4 Stability regions for MIS3Bb with exact integration (*left*) and stepsequence [4, 6, 8] (*right*). Axis are CFL numbers with respect to macro step size Δt

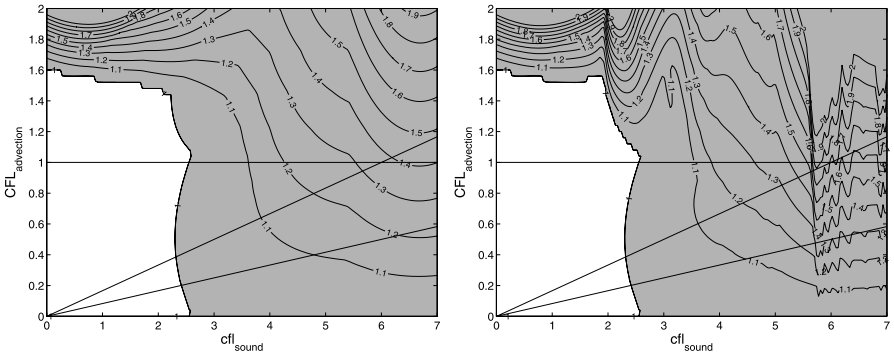

Fig. 5 Stability regions for CF3 with exact integration (*left*) and stepsequence [3, 6, 6] (*right*). Axis are CFL numbers with respect to macro step size Δt

there is more freedom for the construction of stable and consistent methods when divergence damping is used. Nevertheless, the reason for the strong coupling in case of undamped sound waves has not been explained in detail up to now.

For linear acoustics this reduces to the equations

$$u_t + U u_x = -c_s \pi_x + \nu u_{xx}$$
$$\pi_t + U \pi_x = -c_s u_x,$$

with a diffusive parameter $\nu = \alpha \Delta x^2 / \Delta \tau$, where $\Delta \tau$ is the micro step size and α is a parameter with a typical choice of $\alpha = 0.05$. Unfortunately, the multirate infinitesimal step analysis is not applicable to that type of filtering—each wave except the constant wave (wavenumber $k = 0$) is wiped out of the solution.

Nevertheless, in order to have a fair comparison with the established RK3 method, we display here stability regions with respect to divergence damping. We apply divergence damping with $\alpha = 0.05$. In order to determine the number of small steps to

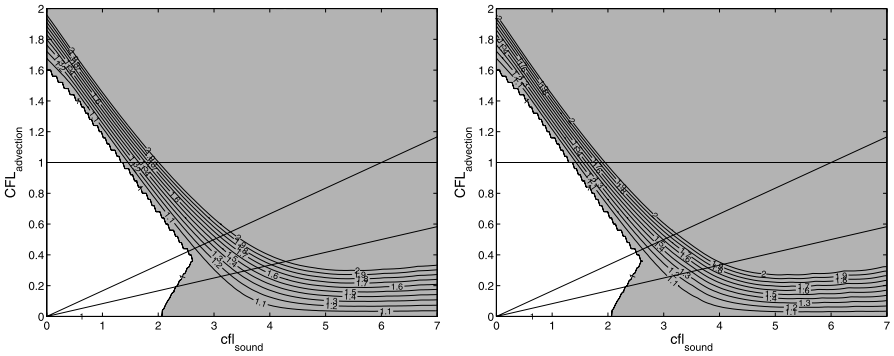

Fig. 6 Stability regions for KW3 with exact integration (*left*) and stepsequence [4, 5, 3] (*right*). Axis are CFL numbers with respect to macro step size Δt

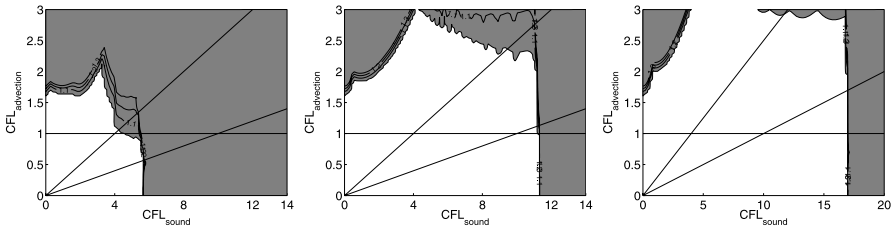

Fig. 7 Stability regions for RK3 with divergence damping, $\alpha = 0.05$, step sequences determined by $C_S \leq 12, 24, 36$. Axis are CFL numbers with respect to macro step size Δt

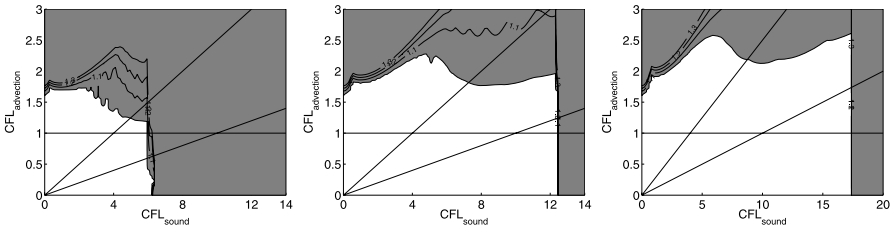

Fig. 8 Stability regions for MIS3A with divergence damping, $\alpha = 0.05$, step sequences determined by $C_S \leq 12, 24, 36$. Axis are CFL numbers with respect to macro step size Δt

be taken we prescribe e maximal CFL number $C_{S,\max} \in \{12, 24, 36\}$ and determine n_i by (5.7).

Below in Figs. 7 to 11 we display the stability regions for RK3, our methods MIS3A and MIS3B as well as CF3 and KW3. The regions are displayed within $(C_A, C_S) \in [0, 3] \times [0, 14]$ in case of $C_{S,\max} \in \{12, 24\}$ and within $(C_A, C_S) \in [0, 3] \times [0, 20]$ in case of $C_{S,\max} = 36$. In addition, the straight lines $C_A = 1$, $C_A = C_S/4$ and $C_A = C_S/10$ are displayed.

All methods except KW3 profit from the divergence damping. For KW3 the bound with respect to advective CFL numbers is to restrictive. Our methods and RK3 are

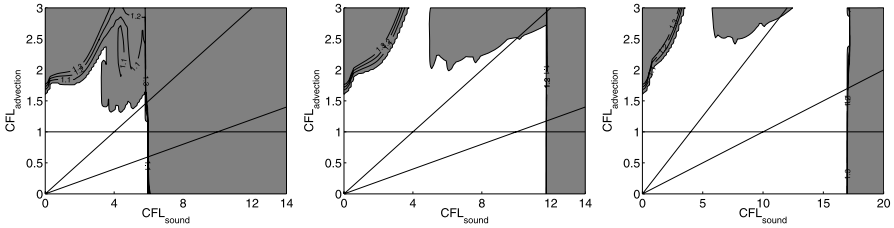

Fig. 9 Stability regions for MIS3B with divergence damping, $\alpha = 0.05$, step sequences determined by $C_S \leq 12, 24, 36$. Axis are CFL numbers with respect to macro step size Δt

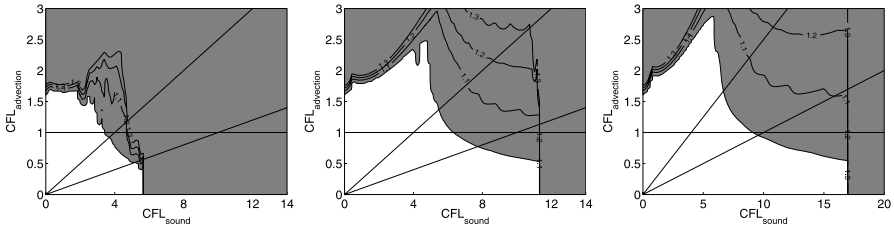

Fig. 10 Stability regions for CF3 with divergence damping, $\alpha = 0.05$, step sequences determined by $C_S \leq 12, 24, 36$. Axis are CFL numbers with respect to macro step size Δt

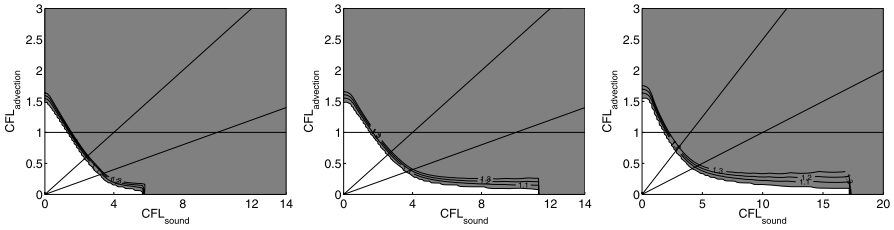

Fig. 11 Stability regions for KW3 with divergence damping, $\alpha = 0.05$, step sequences determined by $C_S \leq 12, 24, 36$. Axis are CFL numbers with respect to macro step size Δt

comparable, whereas our methods perform in the case where C_S is limited by $C_S \leq 12$ even without divergence damping as well as with divergence damping. RK3 needs divergence damping to reach a stability region that covers the C_S-axis up to $C_S \approx 6$.

6 Numerical experiments

We compare the methods MIS3A and MIS3B with RK3 [25], the exponential integrator CF3 [4] and the method of Knoth/Wolke KW3 [13]. We compare accuracy and stability for the linear acoustics equation, and show improved stability properties even for a nonlinear example.

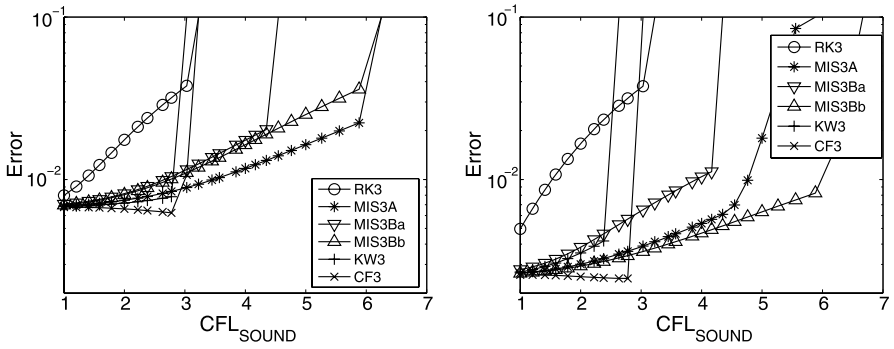

Fig. 12 Error vs. CFL number for $c/U = 12$ (*left*) and $c/U = 6$ (*right*) for the acoustics equation

6.1 Tests on linear acoustics

The 1d linear acoustics problem described in Sect. 5.2 is considered. The problem is spatially discretized in the interval $[-2\pi, 2\pi]$ on an Arakawa-C-grid [1] with 200 points with periodic boundary conditions. We choose the initial profile

$$u(0,x) = \begin{cases} (\cos x + 1)^2 & \text{for } |x| \le \pi, \\ 0 & \text{for } |x| > \pi, \end{cases} \qquad \pi(0,x) = 0.$$

The problem is solved for two different pairs $(c_S, U) = (1, \frac{1}{12})$ and $(c_S, U) = (1, \frac{1}{6})$ in $[0, t_e]$. The macro time steps Δt are chosen such that the resulting macro time step CFL numbers $C_S = c_s \Delta t / \Delta x$ are in the range $[1, 7]$. The end time $t_e = 4\pi/U$ is chosen in such a way, that the exact solution at $t = t_e$ is identical to the initial profile for the first time.

The error measured in the discrete L_2-norm between the numerical solution and the exact solution at $t = t_e$ is plotted vs. the macro time step CFL number C_S in Fig. 12. We point out that the spatial grid remains fixed in our experiments—therefore the numerical solution converges to the exact solution of the semidiscretised problem. For small CFL numbers the error measured is just the difference between the exact solution of the hyperbolic problem and the exact solution of the semidiscretised problem.

We plot the errors in the range $[0, 0.1]$ on a logarithmic scale. The maximum stable CFL numbers are indicated by the first occurrence of solutions with an error larger than 0.1. The theoretically predicted stability bounds on the macro time step CFL numbers can be clearly identified to be between 2 and 3 for RK3, KW3, CF3. Our methods MIS3A and MISBb have a stability bound of 6, whereas for MIS3Ba (using half as much small time steps as MIS3Bb) the stability bound shrinks to 4.5.

Because the different methods use a different number of small time steps, it is interesting to compare error vs. computational effort. Figure 13 shows the comparison of the errors depending on the CPU time. The method CF3 seems to be best for higher accuracies, but for moderate accuracies methods with relaxed stability restrictions such as MIS3A, MIS3Bb have to preferred.

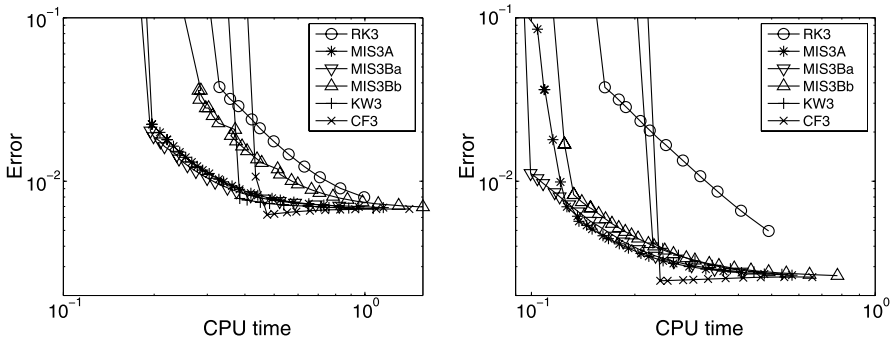

Fig. 13 Error vs. CPU time for $c/U = 12$ (*left*) and $c/U = 6$ (*right*) for the acoustics equation

6.2 Euler equations

In addition experiments are performed with the proposed methods applied to the two–dimensional nonlinear Euler equations

$$\frac{\partial \rho}{\partial t} = -\frac{\partial \rho u}{\partial x} - \frac{\partial \rho w}{\partial z} \tag{6.1a}$$

$$\frac{\partial \rho u}{\partial t} = -\frac{\partial \rho u u}{\partial x} - \frac{\partial \rho w u}{\partial z} - \frac{\partial p}{\partial (\rho\theta)} \frac{\partial (\rho\theta)}{\partial x} \tag{6.1b}$$

$$\frac{\partial \rho w}{\partial t} = -\frac{\partial \rho u w}{\partial x} - \frac{\partial \rho w w}{\partial z} - \frac{\partial p}{\partial (\rho\theta)} \frac{\partial (\rho\theta)}{\partial z} - \rho g \tag{6.1c}$$

$$\frac{\partial \rho\theta}{\partial t} = -\frac{\partial \rho u \theta}{\partial x} - \frac{\partial \rho w \theta}{\partial z} \tag{6.1d}$$

$$p = \rho R \theta (p/p_0)^{\kappa} \tag{6.1e}$$

in height coordinates without orography. Here u denotes the horizontal velocity, w the vertical velocity, ρ the density, θ potential temperature, and p pressure. The primary variables are

$$\begin{pmatrix} U \\ W \\ \Theta \\ \rho \end{pmatrix} = \begin{pmatrix} \rho u \\ \rho w \\ \rho\theta \\ \rho \end{pmatrix}.$$

The spatial discretization uses an Arakawa C-grid with periodic boundary conditions in the horizontal and rigid boundary conditions $w = 0$ at $z = 0$ and $z = H$. Advection terms are discretized by the above mentioned third order upwind method, the pressure term by central differences and the gravity term is averaged from cell center to the face position where the vertical wind component is located.

The example is a strongly numerical flow and describes a rising thermal in an adiabatic atmosphere in a uniform horizontal flow of 20 $\mathrm{m\,s^{-1}}$ with pressure in hydrostatic balance. The initial and the final potential temperature perturbations are

Table 2 Maximal possible time step for the above mentioned methods

Method	RK3	KW3	CF3	MIS3A
Macro Time Step in s	0.9	0.5	0.5	1.6

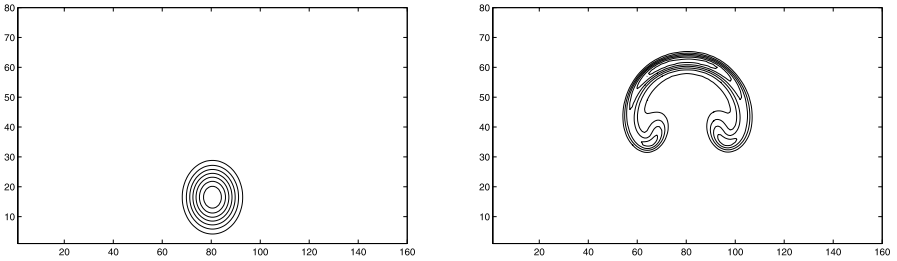

Fig. 14 Thermal bubble at the beginning (*left*) and after 1000 s of simulations (*right*) for the RK3 method

displayed in Fig. 14. The thermal is transported laterally in a horizontally periodic domain while rising upward by buoyancy.

The grid spacing is 125 m in both the x and z directions, and the domain is 20 km wide and 10 km deep. The initial thermal has a radius of 2 km and is placed in the center of the domain at a height of 2 km with a potential temperature excess of 2 K. The solution is integrated for 1000 s, such that the rising thermal should be located in the center of the domain and the solution should remain symmetric, see also Wicker and Skamarock [24]. The terms represented in boldface in (6.1) are treated explicitly in the time integration method and all other terms are part of the fast integration.

We have applied the methods RK3, KW3, CF3 and MIS3A to the problem. Divergence damping is not applied. The macro time step Δt has been chosen maximal such that the final solution remains stable. All 4 methods show qualitatively correct solutions for potential temperature and vertical velocities (displayed in Fig. 15) for this benchmark problem. Whereas in the center region the vertical winds (up to 8 m s^{-1}) are positive, outside of the bubble air flows downwards. Symmetry of the solution is preserved for all 4 methods. The maximal stepsizes are given in Table 2. The linear stability analysis extends well to the nonlinear case—without divergence damping our method MIS3A allows an almost doubled stepsize compared with RK3.

7 Summary and conclusion

We have generalised split-explicit Runge Kutta methods to the class of Multirate Infinitesimal Step methods (MIS). These methods generalise, too, the class of commutator free exponential integrators developed by [4]. Analysis of order and stability is essentially based on the interpretation of the fast component integration procedure being exact. Novel in the concept is the inclusion of previous tendencies (γ-terms) into the righthand side of the fast integration procedure. This additional degree of

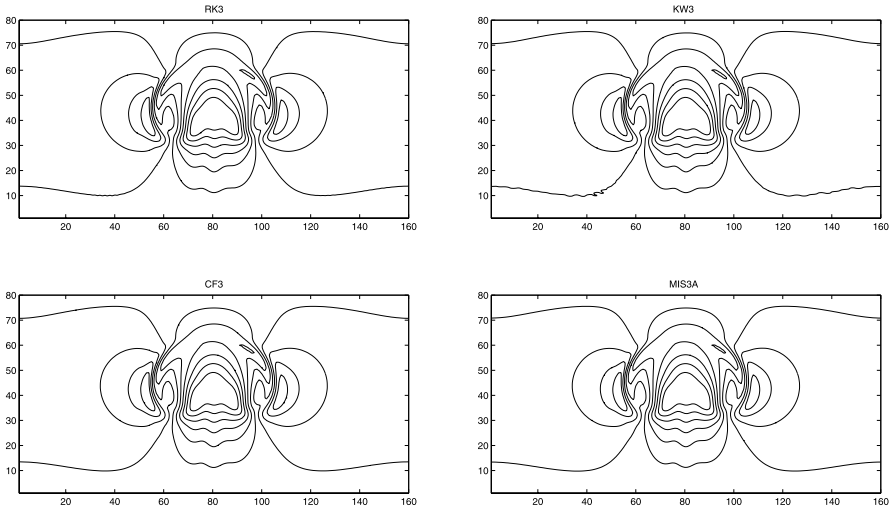

Fig. 15 Contours of vertical wind after 1000 s of simulations for the four methods

freedom allows the construction of methods that allow a stepsize twice as large as for standard partitioned Runge-Kutta methods as well as exponential integrators.

An open question is how to maintain the order of the method when a lower order integration method is used for the fast process integration. In principle, an analysis using asymptotic expansion of the global error of the fast process integration procedure should give restrictions on the stepsize sequences allowed to maintain the order.

Appendix

Coefficients of method MIS3A:

$$\boldsymbol{\alpha} = \left(\begin{array}{ccc} 0.0 & & \\ 0.0 & 0.1262120947528743 & \\ \hline 0.0 & 0.9014049635455670 & -0.1273518110241908 \end{array}\right),$$

$$\boldsymbol{\beta} = \left(\begin{array}{ccc} 0.3798786885245902 & & \\ 0.0734109091499805 & 0.4330940089351694 & \\ \hline -0.0982317605304536 & -0.1550393152471826 & 1.0130284528345010 \end{array}\right),$$

$$\boldsymbol{\gamma} = \left(\begin{array}{ccc} 0.0 & & \\ 0.0 & 0.1499085134212641 & \\ \hline 0.0 & 0.3225318330936224 & -0.2401749994875805 \end{array}\right),$$

$$A = \left(\begin{array}{ccc} 0.3798786885245902 & & \\ 0.1783032436577844 & 0.4330940089351694 & \\ \hline 0.3011845221683809 & -0.3142129750028820 & 1.0130284528345010 \end{array}\right).$$

Coefficients of method MIS3B:

$$\boldsymbol{\alpha} = \left(\begin{array}{lll} 0.0 & & \\ 0.0 & 0.0567447894712588 & \\ \hline 0.0 & 0.5984205948350817 & -0.0761105269067489 \end{array}\right),$$

$$\boldsymbol{\beta} = \left(\begin{array}{lll} 0.4197138394323076 & & \\ 0.0494103174250211 & 0.5761341869014835 & \\ \hline -0.2304896605104612 & 0.4282028054551005 & 0.6892421263984294 \end{array}\right),$$

$$\boldsymbol{\gamma} = \left(\begin{array}{lll} 0.0 & & \\ 0.0 & 0.0784430572133444 & \\ \hline 0.0 & 0.6791817901685916 & -0.5441329940536196 \end{array}\right),$$

$$A = \left(\begin{array}{lll} 0.4197138394323076 & & \\ 0.1061505276016020 & 0.5761341869014835 & \\ \hline 0.2398985647758853 & 0.0708593088256853 & 0.6892421263984294 \end{array}\right).$$

References

1. Arakawa, A.: Computational design for long-term numerical integration of the equations of fluid motion: two-dimensional incompressible flow. Part I. J. Comput. Phys. **135**, 119–143 (1966)
2. Celledoni, E.: Eulerian and semi-Lagrangian schemes based on commutator-free exponential integrators. In: CRM Proc. Lecture Notes: Group Theory and Numerical Analysis, vol. 39, pp. 77–90. Amer. Math. Soc., Providence (2005)
3. Celledoni, E., Kometa, B.K.: Semi-Lagrangian exponential integrators for convection dominated problems. Tech. Report 9/08, Norwegian Institute of Science and Technology (2008). J. Sci. Comput. (to appear)
4. Celledoni, E., Marthinsen, A., Owren, B.: Commutator-free Lie group methods. Future Gener. Comput. Syst. **19**, 341–352 (2003)
5. Durran, D.R.: Improving the anelastic approximation. J. Atmos. Sci. **46**, 1453–1461 (1989)
6. Durran, D.R.: Numerical Methods for Wave Equations in Geophysical Fluid Dynamics. Springer, New York (1999)
7. Gassmann, A.: An improved two-time-level split-explicit integration scheme for non-hydrostatic compressible models. Meteorol. Atmos. Phys. **88**, 23–38 (2005)
8. Gear, C., Wells, R.: Multirate linear multistep methods. BIT **24**, 484–502 (1984)
9. Gill, A.: Atmosphere–Ocean Dynamics. Academic Press, New York (1982)
10. Günther, M., Rentrop, P.: Multirate ROW methods and latency of electric circuits. Appl. Numer. Math. **13**(1–3), 83–102 (1993)
11. Hochbruck, M., Lubich, C.: On Krylov subspace approximations to the matrix exponential operator. SIAM J. Numer. Anal. **34**(5), 1911–1925 (1997)
12. Hochbruck, M., Ostermann, A.: Exponential Runge-Kutta methods for parabolic problems. Appl. Numer. Math. **53**, 323–339 (2005)
13. Knoth, O., Wolke, R.: Implicit–explicit Runge-Kutta methods for computing atmospheric reactive flows. Appl. Numer. Math. **28**, 327–341 (1998)
14. Ogura, Y., Phillips, N.: Scale analysis for deep and shallow convection in the atmosphere. J. Atmos. Sci. **19**, 173–179 (1962)
15. Owren, B.: Order conditions for commutator-free Lie group methods. J. Phys. A **39**, 5585–5599 (2006)
16. Reich, S., Hundertmark, T.: A regularization approach for a vertical slice model and semi-Lagrangian Stormer-Verlet time-stepping. Q. J. R. Meteorol. Soc. **133**, 1575–1587 (2007)
17. Skamarock, W., Klemp, J.B., Dudhia, J., Gill, D.O., Barker, D.M., Wang, W., Powers, J.G.: A description of the advanced research wrf version 2. Tech. Report TN-468, NCAR, Boulder, Colorado (2005)

18. Skamarock, W.C., Klemp, J.B.: The stability of time split numerical methods for the hydrostatic and non-hydrostatic elastic equations. Mon. Weather Rev. **120**, 2109–2127 (1992)
19. Skamarock, W.C., Klemp, J.B.: A time-split nonhydrostatic atmospheric model for weather research and forecasting applications. J. Comput. Phys. **227**, 3465–3485 (2008)
20. Skelboe, S.: Stability properties of backward differentiation multirate formulas. Appl. Numer. Math. **5**, 151–160 (1989)
21. Skelboe, S., Anderson, P.: Stability properties of backward Euler multirate formulas. SIAM J. Sci. Stat. Comput. **10**, 1000–1009 (1989)
22. Strehmel, K.: Stabilitätseigenschaften adaptiver Runge-Kutta-Verfahren. Z. Angew. Math. Mech. **61**, 253–260 (1981)
23. Strehmel, K., Weiner, R.: Behandlung steifer Anfangswertprobleme gewöhnlicher Differentialgleichungen mit adaptiven Runge-Kutta-Methoden. Computing **29**, 153–165 (1982)
24. Wicker, L.J., Skamarock, W.: A time-splitting scheme for the elastic equations incorporating second-order Runge-Kutta time differencing. Mon. Weather Rev. **126**, 1992–1999 (1998)
25. Wicker, L.J., Skamarock, W.: Time splitting methods for elastic models using forward time schemes. Mon. Weather Rev. **130**, 2088–2097 (2002)